Journal of Physics: Conference Series **576** (2015) 012004 doi:10.1088/1742-6596/576/1/012004

Generalized Collisional Radiative Model for Light Elements: C: Data for the B Isonuclear Sequence

S. D. Loch, C. P. Ballance, and M.S. Pindzola
Department of Physics, Auburn University, Auburn, AL 36849

D. C. Griffin
Department of Physics, Rollins College, Winter Park, FL 32789

J. P. Colgan
Los Alamos National Laboratory, Los Alamos, NM 87545

N. R. Badnell and M. G. O'Mullane
Department of Physics, University of Strathclyde, Glasgow, UK G40NG

Abstract. A first stage collision database is assembled which contains electron-impact excitation, ionization, and recombination rate coefficients for B, B^{+}, B^{2+}, B^{3+}, and B^{4+}. The first stage database is constructed using the *R*-matrix with pseudo-states, time-dependent close-coupling, and perturbative distorted-wave methods. A second stage collision database is then assembled which contains generalized collisional-radiative ionization, recombination, and power loss rate coefficients as a function of both temperature and density. The second stage database is constructed by solution of the collisional-radiative equations in the quasi-static equilibrium approximation using the first stage database. Both collision database stages reside in electronic form at the IAEA Labeled Atomic Data Interface (ALADDIN) database and the Atomic Data Analysis Structure (ADAS) open database.

1. Introduction

Accurate atomic and molecular databases underpin current research efforts in a variety of scientific and engineering areas: including controlled fusion energy, astrophysics, radiation biophysics, fluorescent lamps, and atmospheric pollutant removal [1]. For laboratory plasmas boronization has been used for many years, in particular for tokamak facilities, to reduce impurity contamination and increase plasma confinement times [2]. In this paper we report on the construction of an electron-ion collision database for the modelling of boron emission in plasmas, for both fusion and astrophysical applications. We present all the fundamental data, along with a brief description of each dataset, and references to the original calculations from which the data was compiled. The fundamental data has been processed through a collisional-radiative modeling suite of codes [3] to produce coefficients that can be used directly in impurity transport and plasma modeling codes.

The fundamental atomic data has been processed into Generalized Collisional-Radiative (GCR) coefficients. Such GCR coefficients are widely used in impurity transport codes such as DEGAS-2 [4], SOLPS [5], and TRANSP [6]. It has been known for some time that impurity transport codes need to track both the ground and metastable populations in their modeling, and that the role of the excited states should be taken into account. These effects are included in GCR coefficients, which are functions both of electron temperature and density. The importance of such coefficients has been demonstrated on various experiments, including Li transport modeling at DIII-D [7].

In this paper we first describe the electron-impact excitation, ionization, and recombination data that is used to produce the new GCR coefficients for B, a number of questions are then explored using the new data.

A range of theoretical methods are used to calculate the atomic data for this work, with the data being taken from a number of previous papers. Effective collision strengths are obtained from recent R-matrix with pseudo-states (RMPS) calculations of excitation cross sections for B [8], B^+ [9], and B^{4+} [10]. Previously unpublished RMPS calculations of excitation cross sections for B^{2+} and B^{3+} are also used to obtain effective collision strengths.

Ionization rate coefficients are obtained from recent R-matrix with pseudo-states (RMPS) and time-dependent close-coupling (TDCC) calculations [11] of ionization cross sections for ground and excited states of B, B^+, and B^{2+}. The recent RMPS and TDCC calculations [11] compare well with previous RMPS and TDCC calculations for the ground and metastable states of B [12], B^+ [13], and B^{2+} [14]. Ionization rate coefficients are obtained from recent distorted-wave (DW) calculations of ionization cross sections for ground and excited states of B^{3+} and B^{4+}. The recent DW calculations compare well with previous convergent close-coupling (CCC) calculations for the ground and metastable states of B^{3+} [15] and previous RMPS calculations for the ground and metastable states of B^{4+} [16].

Recombination rate coefficients are obtained from previous distorted-wave (DW) calculations for first row ionization states of all atoms [17]; in particular, recombination for Be-like [18], Li-like [19], He-like [20], and H-like [22] atomic ions.

Making use of the complete electron-ion collision database for boron, the collisional-radiative codes found in the Atomic Data and Analysis Structure (ADAS) package [23, 3] are employed to derive Generalized Collisional-Radiative (GCR) and radiated power loss coefficients for the ground and metastable terms of each ionization stage of boron. These generalized collisional-radiative coefficients can be used by subsequent plasma transport codes to track the evolution of the ground and metastable term populations of the B ions. Of particular interest for this study is the role of excited state ionization on the effective ionization rate coefficients. It was previously found for Li that the excited states can increase the effective ionization by up to a factor of 10 over the pure ground state ionization rate coefficient [24]. The current data for B provides a useful opportunity to study the trends of the excited state ionization contribution along an iso-nuclear sequence. For example, at what ion stage does the excited state ionization contribution become negligible? Calculations of ionization cross sections using non-perturbative methods can be very large, so knowing which ion stages and n-shells are the most important for excited state ionization contributions would help to guide future calculations.

The basic collisional rate coefficients and all the ADAS derived generalized collisional-radiative and radiated power loss coefficients are stored in electronic form at the IAEA Labeled Atomic Data Interface (ALADDIN) database [25] and the Atomic Data Analysis Structure (ADAS) open database [26]. The present paper is the third in a series providing generalized collisional-radiative data for the modelling of light species. The first data paper was on lithium [24], the second data paper on beryllium [27], and with work underway on papers for carbon and other light elements.

The remainder of this paper is organized as follows. In Section II we give a brief review of the electron-impact excitation, ionization, and recombination cross sections and rates forming the first stage collision database including references to the original works. In Section III we describe the generalized collisional-radiative data which is generated from the first stage data. In Section IV we investigate the role of excited state ionization on the effective ionization rate coefficients. In Section V we summarize our findings and discuss future directions.

2. First Stage Collision Database

2.1. Electron-Ion Excitation

Effective collision strengths (dimensionless) versus temperatures (in K) are stored in the first stage collision database. The effective collision strengths, obtained by Maxwellian convolution of the cross sections, are given by:

$$\Upsilon_{i\rightarrow f}(T_e) = \int_0^\infty w_i \frac{\epsilon_i}{I_H} \frac{\sigma_{i\rightarrow f}}{\pi a_0^2} e^{-(\frac{\epsilon_f}{kT_e})} d(\frac{\epsilon_f}{kT_e}) \ , \tag{1}$$

where w_i is the statistical weight of the initial LS term, ϵ_i and ϵ_f are initial and final electron energies (in eV), I_H = 13.6 eV, $\sigma_{i\rightarrow f}$ is the excitation cross section (in cm^2), kT_e is the temperature (in eV), and $a_0 = 5.29 \times 10^{-9}$ cm. One can easily transform the stored effective collision strengths into excitation rate coefficients (in cm^3/sec) given by:

$$q_{i\rightarrow f}(T_e) = 2\sqrt{\pi}\alpha c a_0^2 \frac{1}{w_f} \frac{I_H}{kT_e} \Upsilon_{i\rightarrow f}(T_e) \ , \tag{2}$$

where $\alpha = 1/137$ and $c = 3.0 \times 10^{10}$ cm/sec. The effective collision strengths, rather than the rate coefficients, are archived as they are slowly varying and easily interpolated. Considering each of the B ions in turn, we briefly describe the calculations that were used to produce the excitation cross sections.

For neutral B, excitation cross sections for the 55 transitions among 11 of the 13 LS terms of the $1s^22s^22p$, $1s^22s2p^2$, $1s^22s^23l$ (l=0-2) $1s^22s^24l$ (l=0-3), and $1s^22s^25s$ configurations were calculated using the RMPS method. The 640 LS term RMPS calculation [8] involved the $1s^22s^2nl$ (n=2-11, l=0-4), $1s^22s2pnl$ (n=2-11, l=0-4), and $1s^22p^2nl$ (n=2-11, l=0-3) configurations. As shown in Figure 1 for the $1s^22p^22p$ (^2P) $\rightarrow$ $1s^22s^23s$ (^2S) transition and in Figure 2 for the $1s^22s2p^2$ (^4P) $\rightarrow$ $1s^22s^23d$ (^2D) transition, the 640 LS term RMPS cross sections are slightly lower than previous smaller RMPS calculations [28] and do not show the pseudoresonance problems above (see Figure 1) and straddling (see Figure 2) the ionization threshold. Effective collision strengths at 8 temperatures from 4,000 K to 50,000 K were obtained using Eq.(1) for all 55 transitions and are found in the first stage electronic collision databases.

For B$^+$, excitation cross sections for the 190 transitions among the 20 LS terms of the $1s^22s^2$, $1s^22s2p$, $1s^22p^2$, $1s^22s3l$ (l=0-2), and $1s^22s4l$ (l=0-3) configurations were calculated using the RMPS method. The 114 LS term RMPS calculation [9] involved the $1s^22snl$ (n=2-10, l=0-4) and $1s^22pnl$ (n=2-5, l=0-4) configurations. The study [9] compared this 114 LS term calculation with a 134 LS term calculation [9], showing little difference in the cross sections, demonstrating convergence in the pseudostate expansion. The 134 LS term RMPS calculation [9] included additional $1s^22snl$ (n=11-12, l=0-4) configurations. Effective collision strengths at 10 temperatures from 800 K to 800,000 K were obtained using Eq.(1) for all 190 transitions and are found in the first stage electronic collision database.

For B^{2+}, excitation cross sections for the 36 transitions among the 9 LS terms of the $1s^22s$, $1s^22p$, $1s^23l$ (l=0-2), and $1s^24l$ (l=0-3) configurations were calculated using

the RMPS method. The 41 LS term RMPS calculation involved the $1s^2nl$ (n=2-12, l=0-3) configurations. The same RMPS calculations were reported for other members of the Li isonuclear sequence [29]. Effective collision strengths at 12 temperatures from 1,800 K to 9,000,000 K were obtained using Eq.(1) for all 36 transitions and are found in the first stage electronic collision database.

For B^{3+}, excitation cross sections for the 171 transitions among the 19 LS terms of the $1s^2$, $1s2s$, $1s2p$, $1s3l$ (l=0-2), and $1s4l$ (l=0-3) configurations were calculated using the RMPS method. The 89 LS term RMPS calculation involved the $1s^2$ and $1snl$ (n=2-11, l=0-4) configurations. Effective collision strengths at 10 temperatures from 16,000 K to 16,000,000 K were obtained by using Eq.(1) for all 171 transitions and are found in the first stage electronic collision database. These calculations were performed for the ADAS database, but are previously unpublished.

For B^{4+}, excitation cross sections for the 105 transitions among the 15 LS terms of the $1s$, $2s$, $2p$, $3l$ (l=0-2), $4l$ (l=0-3), and $5l$ (l=0-4) configurations were calculated using the RMPS method. The 39 LS term RMPS calculation [10] involved the $1s$ and nl (n=2-9, l=0-5) configurations. Effective collision strengths at 12 temperatures from 50,000 K to 12,500,000 K were obtained by using Eq.(1) for all 105 transitions and are found in the first stage electronic collision database.

2.2. Electron-Ion Ionization

Scaled ionization rate coefficients (in cm^3/sec) versus temperatures (in K) are stored in the first stage collision database. The scaled ionization rate coefficients are given by:

$$\bar{S}_{i\to f}(T_e) = \mathscr{S}_{i\to f}(T_e)e^{-(\frac{I_p}{kT_e})} \ , \tag{3}$$

where I_p is the ionization potential (in eV) of the level being ionized (i.e. not simply the ionization potential of the ground state). Ionization rate coefficients are given by:

$$\mathscr{S}_{i\to f}(T_e) = \frac{2\alpha c}{\sqrt{\pi}}(\frac{1}{I_H})^{\frac{1}{2}}(\frac{1}{kT_e})^{\frac{3}{2}}\int_{I_p}^{\infty}\epsilon_i\sigma_{i\to f}e^{-(\frac{\epsilon_i}{kT_e})}d\epsilon_i \ , \tag{4}$$

where $\sigma_{i\to f}$ is the ionization cross section (in cm^2). The scaled ionization rate coefficients are stored since they are more easily interpolated than the rate coefficients, particularly at low temperatures. We briefly describe here the sources and methods used for the ionization data.

For neutral B, ionization cross sections for the 8 LS terms of the $1s^22s^22p$, $1s^22s^23l$ (l=0-2), and $1s^22s^24l$ (l=0-3) configurations were calculated using the RMPS method. The 1036 LS term RMPS calculation [11] involved the $1s^22s^22p$, $1s^22s^2nl$ (n=3-13, l=0-5), $1s^22s2p^2$, $1s^22s2pnl$ (n=3-13, l=0-5), $1s^22p^3$, and $1s^22p^2nl$ (n=3-13, l=0-5) configurations. The $1s^22s^22p$ (^2P) cross sections are in good agreement with previous 476 LS term RMPS and TDCC calculations [12]. As shown in Figure 3 for the ionization of the 7 LS terms of the $1s^22s^23l$ and $1s^22s^24l$ configurations, the RMPS calculations for the $1s^22s^23s$ (^2S) term are in good agreement with TDCC calculations [11]. Scaled ionization rate coefficients at 8 temperatures from 4,000 K to 50,000 K were obtained using Eqs.(3)-(4) for all 8 LS terms and are found in the first stage electronic collision database.

For B^+, ionization cross sections for the 17 LS terms of the $1s^22s^2$, $1s^22s2p$, $1s^22s3l$ (l=0-2), and $1s^22s4l$ (l=0-3) configurations were calculated using the RMPS method. The 486 LS term RMPS calculation [11] involved the $1s^22s^2$, $1s^22s2p$, $1s^22snl$ (n=3-14, l=0-5), $1s^22p^2$, and $1s^22pnl$ (n=3-14, l=0-5) configurations. The $1s^22s^2$ (^1S) cross sections are in good agreement with previous 414 LS term RMPS and TDCC calculations [13]. Scaled ionization rate coefficients at 10 temperatures from 800 K to 800,000 K were obtained using Eqs.(3)-(4) for all 17 LS terms and are found in the first stage electronic collision database.

For B^{2+}, ionization cross sections for the 14 LS terms of the $1s^22s$, $1s^22p$, $1s^23l$ (l=0-2), $1s^24l$ (l=0-3), and $1s^25l$ (l=0-4) configurations were calculated using the RMPS method. The 68 LS term RMPS calculation [11] involved the $1s^22s$, $1s^22p$, and $1s^2nl$ (n=3-14, l=0-5) configurations. The $1s^22s$ ^2S cross sections are in good agreement with previous 68 LS term RMPS and TDCC calculations [14]. Scaled ionization rate coefficients at 12 temperatures from 1,800 K to 9,000,000 K were obtained using Eqs.(3)-(4) for all 14 LS terms and are found in the first stage electronic collision database.

For B^{3+}, ionization cross sections for the 19 LS terms of the $1s^2$, $1s2s$, $1s2p$, $1s3l$ (l=0-2), and $1s4l$ (l=0-3) configurations were calculated using the DW method. The $1s^2$

and $1s2s\ ^3S$ cross sections are in good agreement with previous CCC calculations [15]. Scaled ionization rate coefficients at 10 temperatures from 16,000 K to 16,000,000 K were obtained using Eqs.(3)-(4) for all 19 LS terms and are found in the first stage electronic collision database.

For B^{4+}, ionization cross sections for the 15 LS terms of the $1s$, $2s$, $2p$, $3l$ (l=0-2), $4l$ (l=0-3), and $5l$ (l=0-4) configurations were calculated using the DW method. The $1s$ and $2l$ (l=0-1) cross sections are in good agreement with previous RMPS calculations [16]. Scaled ionization rate coefficients at 12 temperatures from 50,000 K to 12,500,000 K were obtained using Eqs.(3)-(4) for all 15 LS terms and are found in the first stage electronic collision database.

Note that DW cross sections are used for ion stages B^{3+} and B^{4+}. It is well known that DW calculations become increasingly appropriate with charge state, while at the same time they may become inaccurate with increasing n-shell. It was not clear which of these two effects dominates along a sequence. However, recently calculations on the excited states of C^{3+} [21] show that DW calculations are valid for ionization from the 5s subshell. Thus, we expect that DW calculations should be appropriate for both the ground and excited states of B^{3+} and B^{4+}.

As part of the set of nonperturbative calculations for B, B^+, and B^{2+}, the possibility of n-scaling the low n-shell data to higher n-values was investigated. For all of the ions it was discovered that the bundled-n data converged onto an n^4-scaling, see Figure 4. The aim in the extrapolation is to provide recommended rates for the higher n-shells present in the projection matrix part of the collisional-radiative modeling, see Section 2.4 for a description of the projection matrix. The projection matrix data uses n-shell resolved data, separated by the spin of the parent, the bundled-nS approach. Note that applying the n^4 scaling is a little more subtle for ion stages that have more than one spin system, in which case one should extrapolate data based upon each spin system separately, see [11] for more details. For example, in B^+ one would n-scale the triplet states separately from the singlet states. This is consistent with the bundled-nS data used in the projection matrix.

2.3. Electron-Ion Recombination

For each of the B ions, the dielectronic recombination (DR) Maxwellian rate coefficients have aleady been calculated as part of the DR project [17]. Our final recommended recombination data consists of this DR data combined with radiative recombination rate coefficients.

Dielectronic recombination rate coefficients (in cm^3/sec) versus temperatures (in K) are stored in the first stage collision database. The Maxwellian recombination rate coefficients are given by:

$$\mathscr{R}_{i\rightarrow f}(T_e) = \frac{2\alpha c}{\sqrt{\pi}}(\frac{1}{I_H})^{\frac{1}{2}}(\frac{1}{kT_e})^{\frac{3}{2}}\int_0^\infty \epsilon_i \sigma_{i\rightarrow f} e^{-(\frac{\epsilon_i}{kT_e})} d\epsilon_i \ , \tag{5}$$

where $\sigma_{i\rightarrow f}$ is the recombination cross section (in cm^2). The recombination rate coefficients generally vary smoothly with temperature.

Dielectronic recombination cross sections for 11 of the 13 LS terms of the $1s^22s^22p$, $1s^22s2p^2$, $1s^22s^23l$ (l=0-2), $1s^22s^24l$ (l=0-3), and $1s^22s^25s$ configurations of B coming from the $1s^22s^2\ ^1S$ and $1s^22s2p\ ^3P$ terms of B^+ were calculated [18] using the DW method. Recombination rate coefficients at 8 temperatures from 4,000 K to 50,000 K were obtained using Eq.(5) for all 22 transitions and are found in the first stage electronic collision databases.

Dielectronic recombination cross sections for the 20 LS terms of the $1s^22s^2$, $1s^22s2p$, $1s^22p^2$, $1s^22s3l$ (l=0-2), and $1s^22s4l$ (l=0-3) configurations of B^+ coming from the $1s^22s\ ^2S$ term of B^{2+} were calculated [19] using the DW method. Recombination rate coefficients at 10 temperatures from 800 K to 800,000 K were obtained using Eq.(5) for all 20 transitions and are found in the first stage electronic collision databases.

Dielectronic recombination cross sections for the 9 LS terms of the $1s^22s$, $1s^22p$, $1s^23l$ (l=0-2), and $1s^24l$ (l=0-3) configurations of B^{2+} coming from the $1s^2\ ^1S$ and $1s2s\ ^3S$ terms of B^{3+} were calculated [20] using the DW method. Recombination rate coefficients at 12 temperatures from 1,800 K to 9,000,000 K were obtained using Eq.(5) for all 18 transitions and are found in the first stage electronic collision databases.

Dielectronic recombination cross sections for the 19 LS terms of the $1s^2$, $1s2s$, $1s2p$, $1s3l$ (l=0-2), and $1s4l$ (l=0-3) configurations of B^{3+} coming from the $1s\ ^2S$ term of B^{4+} were calculated [22] using the DW method. Recombination rate coefficients at 10 temperatures from 16,000 K to 16,000,000 K were obtained using Eq.(5) for all 19 transitions and are found in the first stage electronic collision databases.

For all ions, radiative recombination was calculated using a Gaunt factor approach [30]. RR rate coefficients were evaluated for the same LS terms as those calculated for the DR calculations described above, and were on the same temperature grid.

For B^{5+} recombining to B^{4+} only radiative recombination is possible. Thus, the Gaunt factor calculations included recombination into the 15 LS terms of the $1s$, $2s$, $2p$, $3l$ (l=0-2), $4l$ (l=0-3), and $5l$ (l=0-4) configurations of B^{4+}. Recombination rate coefficients at 12 temperatures from 50,000 K to 12,500,000 K were obtained using Eq.(5)

for all 15 transitions and are found in the first stage electronic collision databases.

Note that three-body recombination can be calculated from the electron-impact ionization rate coefficients using the detailed balance relations, and so is included in our collisional-radiative modeling.

2.4. Hign n-Shell Data

As with our previously published Li [24] and Be [27] datasets, we included approximate atomic data for high n-shells. It can be important to include data for these higher n-shells for a number of reasons. Under low temperature or higher density conditions, the total ionization losses from an ion stage can be dominated by stepwise ionization and inclusion of these higher n-shells in the population modelling becomes important. Also, at low densities dielectronic recombination into the higher n-shells is a strong populating mechanism, and must be accounted for.

Our high n-shell data is included through the use of a projection matrix. Our data consists of semi-empirical expressions, based on the Gaunt factor and ECIP expressions of Burgess and Summers [30]. For B, B^+, and B^{2+} we use the scaled R-matrix ionization rate coefficients as described in Section 2.2. We note that the dielectronic recombination data in our projection matrix data is based on the ICDW calculations reported in Section IIC, and as such are the only part of the projection matrix data that is not semi-empirical or n-scaled.

3. Second Stage Collision Database

The first stage atomic collision data presented in Section II can be used directly to calculate term populations via the collisional-radiative equations:

$$\begin{aligned}\frac{dN_j^z}{dt} = & -\sum_{j'<j} A_{j\to j'} N_j^z - N_e \sum_{j'\neq j} q_{j\to j'} N_j^z \\ & + \sum_{j'>j} A_{j'\to j} N_{j'}^z + N_e \sum_{j'\neq j} q_{j'\to j} N_{j'}^z \\ & - N_e \sum_k \mathscr{S}_{j\to k} N_j^z + N_e \sum_k \mathscr{R}_{k\to j} N_k^{z+1} \ , \end{aligned} \tag{6}$$

where $A_{j\to j'}$ are radiative decay rates, $\mathscr{S}_{j\to k}$ are electron-impact ionization rates, $\mathscr{R}_{k\to j}$ are electron-impact recombination rates, and N_e is the electron density. The electron-impact excitation rates, $q_{i\to j}$, are proportional [14] to the effective collision strengths.

For many plasma conditions, the ground and metastable term populations evolve on a much slower timescale than the excited term populations, allowing the time derivative of the excited term populations to be set to zero. In the quasi-static equilibrium approximation, the time-dependence of the excited states are set to zero and one can extract generalized coefficients that connect the ground and metastable states for each ion stage. These generalized coefficients can be used to evaluate a time-dependent ionization balance, as shown in Eq. (7), or can be used directly in plasma transport codes. As an illustrative example, consider the connections between three adjacent ion stages, labelled α, β, and γ. Each ion stage has metastable states, given by α', β', and γ'. The center ion stage (with β and β') contains excited states given by j and j'. The time-dependence of the ground state β can be calculated from:

$$\begin{aligned}\frac{dN_\beta^z}{dt} = & -N_e \sum_{\beta'\neq\beta} (X_{\beta\to\beta'} + Q_{\beta\to\beta'}) N_\beta^z \\ & + N_e \sum_{\beta'\neq\beta} (X_{\beta'\to\beta} + Q_{\beta'\to\beta}) N_{\beta'}^z \\ & - N_e \sum_\gamma S_{\beta\to\gamma} N_\beta^z + N_e \sum_\alpha S_{\alpha\to\beta} N_\alpha^{z-1} \\ & + N_e \sum_\gamma R_{\gamma\to\beta} N_\gamma^{z+1} - N_e \sum_\alpha R_{\beta\to\alpha} N_\beta^z \ . \end{aligned} \tag{7}$$

The cross-coupling rate coefficients are given by:

$$X_{\beta\to\beta'} = (\mathcal{C}_{\beta'\beta}^z - \sum_j \mathcal{C}_{\beta' j}^z \sum_{j'} (\mathcal{C}_{jj'}^z)^{-1} \mathcal{C}_{j'\beta}^z)/N_e, \tag{8}$$

and the parent cross-coupling rate coefficients are given by:

$$Q_{\beta\to\beta'} = N_e \sum_i \mathscr{S}_{i\to\beta'} \sum_{i'} (\mathcal{C}_{ii'}^{z-1})^{-1} \mathscr{R}_{\beta\to i'} \ , \tag{9}$$

where the collisional-radiative matrix elements for ion stage z are given by:

$$\mathcal{C}_{jj}^z = \sum_{j'<j} A_{j\to j'} + N_e \sum_{j'\neq j} q_{j\to j'}, \tag{10}$$

$$\mathcal{C}^z_{jj'} = -A_{j'\to j} - N_e q_{j'\to j} \qquad for \quad j' > j, \tag{11}$$

$$\mathcal{C}^z_{jj'} = -N_e q_{j'\to j} \qquad for \quad j' < j. \tag{12}$$

The generalized ionization rate coefficients are given by:

$$S_{\beta\to\gamma} = \mathscr{S}_{\beta\to\gamma} - \sum_j \mathscr{S}_{j\to\gamma} \sum_{j'} (\mathcal{C}^z_{jj'})^{-1} \mathcal{C}^z_{j'\beta}, \tag{13}$$

$$S_{\alpha\to\beta} = \mathscr{S}_{\alpha\to\beta} - \sum_i \mathscr{S}_{i\to\beta} \sum_{i'} (\mathcal{C}^{z-1}_{ii'})^{-1} \mathcal{C}^{z-1}_{i'\alpha}. \tag{14}$$

The generalized recombination rate coefficients are given by:

$$R_{\gamma\to\beta} = \mathscr{R}_{\gamma\to\beta} - \sum_j \mathcal{C}^z_{\beta j} \sum_{j'} (\mathcal{C}^z_{jj'})^{-1} \mathscr{R}_{\gamma\to j'}, \tag{15}$$

$$R_{\beta\to\alpha} = \mathscr{R}_{\beta\to\alpha} - \sum_i \mathcal{C}^{z-1}_{\alpha i} \sum_{i'} (\mathcal{C}^{z-1}_{ii'})^{-1} \mathscr{R}_{\beta\to i'}. \tag{16}$$

These generalized collisional-radiative coefficients are a function of both temperature and density. Consider for example Eqn (13) and the effective ionization from β to γ. The GCR ionization rate coefficient includes both the direct ionization from β to γ, as well as excited state ionzization (i.e. collisional-excitation fromβ to j', collisional redistribution to j and then ionization from j).

Our second stage database contains the generalized collisional-radiative coefficients for all of the B ion stages. We note that it is these generalized collisional-radiative coefficients that are most useful in plasma transport codes, since they contain the effects of the excited states on the ground and metastables, without the need for a large number of coefficients to be archived.

To illustrate the role of excited state ionization on the B ions, we show a comparison of the ground state ionization rate coefficient with the effective ionization rate coefficient at an electron density of N_e=1$\times$ 10^{14}cm^{-3}. Figure 5 shows the absolute ionization rate coefficient for neutral B. Figure 6 shows the ratio of the ground state ionization rate coefficient to the GCR ionization rate coefficient calculated at N_e=1$\times$ 10^{14}cm^{-3} for the first three charge states of B. We show the results here using just the low-n data (i.e. no projection matrix) to highlight the sensitivity of the GCR coefficients to the non-perturbative rate coefficients calculated as part of this work. We have chosen a typical density for a tokamak divertor plasma ($N_e = 1\times10^{14}$ cm^{-3}) and an electron temperature at the lower range of expected divertor conditions ($T_e = 1$ eV), as representative of the types of conditions that B ions sputtered into the divertor region might experience. For neutral B, the excited terms contribute up to a factor of 10 more than the ground state, similar to previous findings for neutral Li [24]. For B^+ the excited states contribute about 20% to the total ionization rate and for B^{2+} the effect is less than 5%. As one would expect, due to the increasing radiative rates, the role of the excited states is becoming less pronounced as one progresses to the higher charge states. For charge states greater than B^{2+}, the excited states do not contribute significantly to the effective

ionization rate coefficient. We note that these effects become larger for higher densities or for lower temperatures, as one might expect.

As a final consideration, we discuss briefly the role of uncertainties on our atomic data. Assigning uncertainties to the final GCR coefficients is a complex problem, as the uncertainties on the fundamental cross section data carry through the collisional-radiative modeling to the final temperature and density dependent coefficients. However, the uncertainties in the fundamental cross sections could be estimated from the spread of non-perturbative cross section data for each of the atomic processes considered here. Inspection of the B ionization cross section papers shows that the TDCC, RMPS and CCC data are usually within 15% of each other for ionization cross sections. Uncertainties on the excitation and recombination cross sections are more difficult to estimate, due to the important role of resonant processes. Clearly the uncertainties will be largest at the lowest temperatures and reduce as the temperature increases. A systematic method to generate uncertainties on excitation and recombination data is currently under development. We note that once uncertainties are assigned to the excitation, ionization and recombination rate coefficients, a Monte-Carlo method can be used to propagate those uncertainties through to uncertainties on the final GCR coefficients.

4. Radiated Power Loss

The radiated power loss function from a single excited term, due to all possible bound-bound spectral line emissions, is given by:

$$RPL_j^z = \sum_{j'<j} \frac{A^z_{j\rightarrow j'} \Delta E^z_{jj'} N^z_j}{N_e N_{tot}} \ , \tag{17}$$

where $\Delta E^z_{jj'}$ is the transition energy. On the other hand, the total radiated power loss function from an ionization stage, due to spectral line emission, is given by:

$$RPL^z = \sum_{\beta} \frac{P^z_{exc,\beta} N^z_\beta}{N_{tot}} + \sum_{\gamma} \frac{P^z_{rec,\gamma} N^{z+1}_\gamma}{N_{tot}} \ . \tag{18}$$

Note that to use this last equation, one needs to know the fractional abundances of each of the ion stages, either from an ionization balance calculation, or from an impurity transport calculation. The generalized excitation power loss coefficients are given by:

$$P^z_{exc,\beta} = \sum_j \sum_{j'<j} \frac{A^z_{j\rightarrow j'} \Delta E^z_{jj'}}{N_e} \left[- \sum_{j''} \mathcal{C}^{-1}_{jj''} \mathcal{C}_{j''\beta} \right] \ , \tag{19}$$

and the generalized recombination power loss coefficients are given by:

$$P^z_{rec,\gamma} = \sum_j \sum_{j'<j} \frac{A^z_{j\rightarrow j'} \Delta E^z_{jj'}}{N_e} \left[N_e \sum_{j''} \mathcal{C}^{-1}_{jj''} \mathscr{R}_{j''\gamma} \right] \ . \tag{20}$$

The power loss coefficients for all charge states of B are also archived as part of this work.

5. Summary

An atomic collision dataset for boron is presented consisting of the highest quality data available for electron impact excitation, ionization and recombination. We used RMPS data for excitation, RMPS, TDCC, and DW data for ionization, and DW data for recombination. For processes involving higher n-shells, we used various approximate expressions for the excitation, ionization and recombination processes, including an extrapolation of the lower n-shell ionization data for B, B+, and B^{2+}. As well as presenting the fundamental data, we have presented the derived atomic coefficients necessary to calculate ionization balance and radiative power loss. These coefficients are referred to as generalized collisional-radiative and radiated power loss coefficients. The first and second stage collision databases will be archived in electronic form at the IAEA/ALADDIN database [25] and the ADAS open database [26].

References

[1] *Atomic and Molecular Data and Their Applications*, editors: D. R. Schultz, P. S. Krstic, and F. Ownby, AIP Conference Proceedings **636**, 2002.
[2] J. WInter, Plasma Physics and Controlled Fusion, **38** 1503 (1996)
[3] *The ADAS User Manual*, H. P. Summers (2001), *http://adas.phys.strath.ac.uk*
[4] D.P. Stotler, CFF. Karney, Contrib. Plasma Phys. **34** 392 (1994)
[5] http://www.ipp.mpg.de/∼dcp/solps.html
[6] http://w3.pppl.gov/transp/
[7] J.P. Allain, D.G. Whyte, and J.N. Brooks, Nucl. Fusion **44**, 655 (2004).
[8] C. P. Ballance, D. C. Griffin, K. A. Berrington, and N. R. Badnell, J. Phys. B **40**, 1131 (2007).
[9] N. R. Badnell, D. C. Griffin, and D. M. Mitnik, J. Phys. B **36**, 1337 (2003).
[10] C. P. Ballance, N. R. Badnell, and E. S. Smyth, J. Phys. B **36**, 3707 (2003).
[11] T. G. Lee, S. D. Loch, C. P. Ballance, J. A. Ludlow, and M. S. Pindzola, Phys. Rev. A **82**, 042721 (2010).
[12] J. C. Berengut, S. D. Loch, M. S. Pindzola, C. P. Ballance, and D. C. Griffin, Phys. Rev. A **76**, 042704 (2007).
[13] J. C. Berengut, S. D. Loch, M. S. Pindzola, C. P. Ballance, D. C. Griffin, M. Fogle, and M. E. Bannister, Phys. Rev. A **78**, 012704 (2008).
[14] O. Woitke, N. Djuric, G. H. Dunn, M. E. Bannister, A. C. H. Smith, B. Wallbank, N. R. Badnell, and M. S. Pindzola, Phys. Rev. A **58**, 4512 (1998).
[15] A. C. Renwick, I. Bray, D. V. Fursa, J. Jacobi, S. Schippers, and A. Muller, J. Phys. B **42**, 175203 (2009).
[16] D. C. Griffin, C. P. Ballance, M. S. Pindzola, F. Robicheaux, S. D. Loch, J. A. Ludlow, M. C. Witthoeft, J. Colgan, C. J. Fontes, and D. R. Schultz, J. Phys. B **38**, L199 (2005).
[17] N. R. Badnell, M. G. O'Mullane, H. P. Summers, Z. Altun, M. A. Bautista, J. Colgan, T. W. Gorczyca, D. M. Mitnik, M. S. Pindzola, and O. Zatsarinny, Astronomy and Astrophysics **406**, 1151 (2003).
[18] J. Colgan, M. S. Pindzola, A. D. Whiteford, and N. R. Badnell, Astronomy and Astrophysics **412**, 597 (2003).
[19] J. Colgan, M. S. Pindzola, and N. R. Badnell, Astronomy and Astrophysics **417**, 1183 (2004).
[20] M. A. Bautista and N. R. Badnell, Astronomy and Astrophysics **466**, 755 (2007).
[21] M. S. Pindzola, C. P. Ballance, and S. D. Loch, Phys. Rev. A **83**, 062705 (2011)
[22] N. R. Badnell, Astronomy and Astrophysics **447**, 389 (2006).

[23] H.P. Summers, W.J. Dickson, M.G. O'Mullane, N.R.Badnell, A.D. Whiteford, D.H. Brooks, J. Lang, S.D. Loch, and D.C. Griffin, Plasma Phys. Control. Fusion **48**, 263 (2006).
[24] S. D. Loch, J. Colgan, M. C. Witthoeft, M. S. Pindzola, C. P. Ballance, D. M. Mitnik, D. C. Griffin, M. G. O'Mullane, N. R. Badnell, and H. P. Summers, Atomic Data and Nuclear Data Tables **92**, 813 (2006).
[25] IAEA/ALADDIN, *www-amdis.iaea.org/aladdin*
[26] EU/ADAS, *www.adas.ac.uk/openadas*
[27] S. D. Loch, M. S. Pindzola, C. P. Ballance, D. C. Griffin, J. Colgan, N. R. Badnell, M. G. O'Mullane, and H. P. Summers, Atomic Data and Nuclear Data Tables **94**, 257 (2008).
[28] P. J. Marchalant and K. Bartschat, J. Phys. B **30**, 4373 (1997).
[29] D. C. Griffin, N. R. Badnell, and M. S. Pindzola, J. Phys. B **33**, 1013 (2000).
[30] A. Burgess and H.P. Summers, Mon. Not. R. Astr. Soc. **174**, 345 (1976).

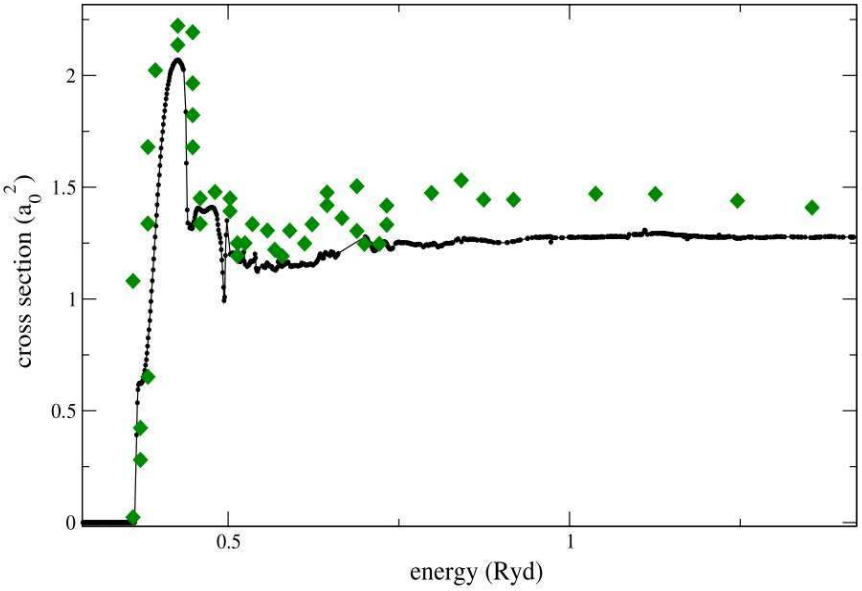

Figure 1. Excitation cross sections for the $1s^2 2s^2 2p\ (^2P) \rightarrow 1s^2 2s^2 3s\ (^2S)$ transition in B. Solid line: RMPS method [8], diamonds: RMPS method [28] (1.0 $a_0^2 = 2.80 \times 10^{-17}$ cm^2 and 1.0 Ryd = 13.6 eV). Figure taken from [8]

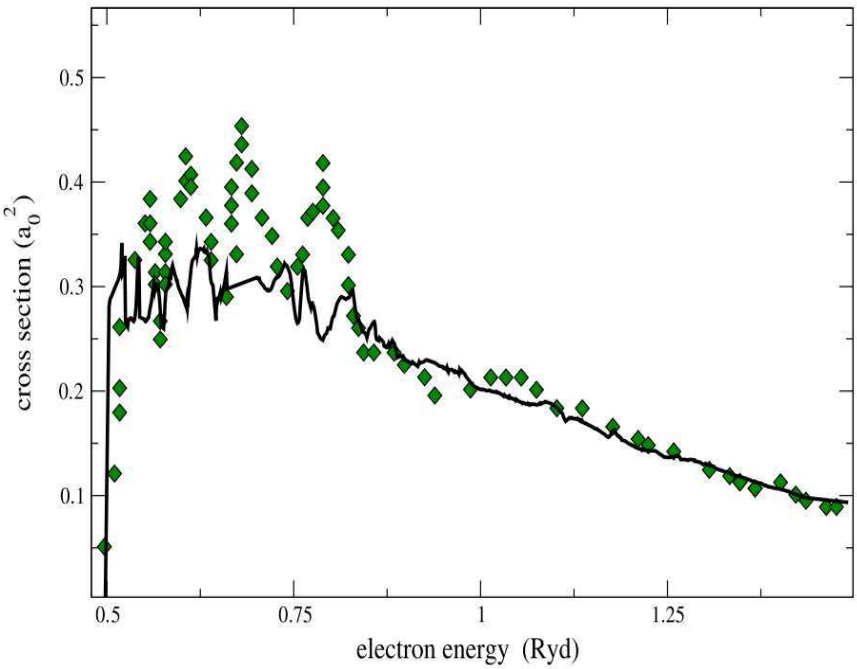

Figure 2. Excitation cross sections for the $1s^2 2s 2p^2\ (^4P) \rightarrow 1s^2 2s^2 3d\ (^2D)$ transition in B. Solid line: RMPS method [8], diamonds: RMPS method [28] (1.0 $a_0^2 = 2.80 \times 10^{-17}$ cm^2 and 1.0 Ryd = 13.6 eV). Figure taken from [8]

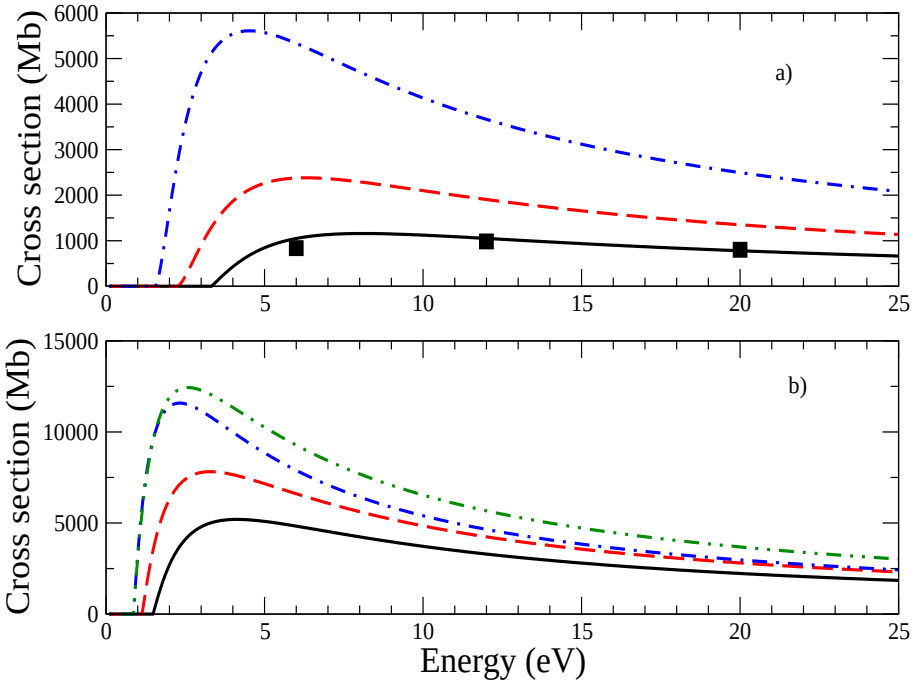

Figure 3. Ionization cross sections for the nl excited states of B. All RMPS and TDCC data are taken from [11]. (a) Solid line: RMPS method for $3s$, dashed line: RMPS method for $3p$, dot-dashed line: RMPS method for $3d$, solid squares: TDCC method for $3s$. (b) Solid line: RMPS method for $4s$, dashed line: RMPS method for $4p$, dot-dashed line: RMPS method for $4d$, double-dot dashed line: RMPS method for $4f$ (1.0 Mb = 1.0×10^{-18} cm^2). Figure taken from [11]

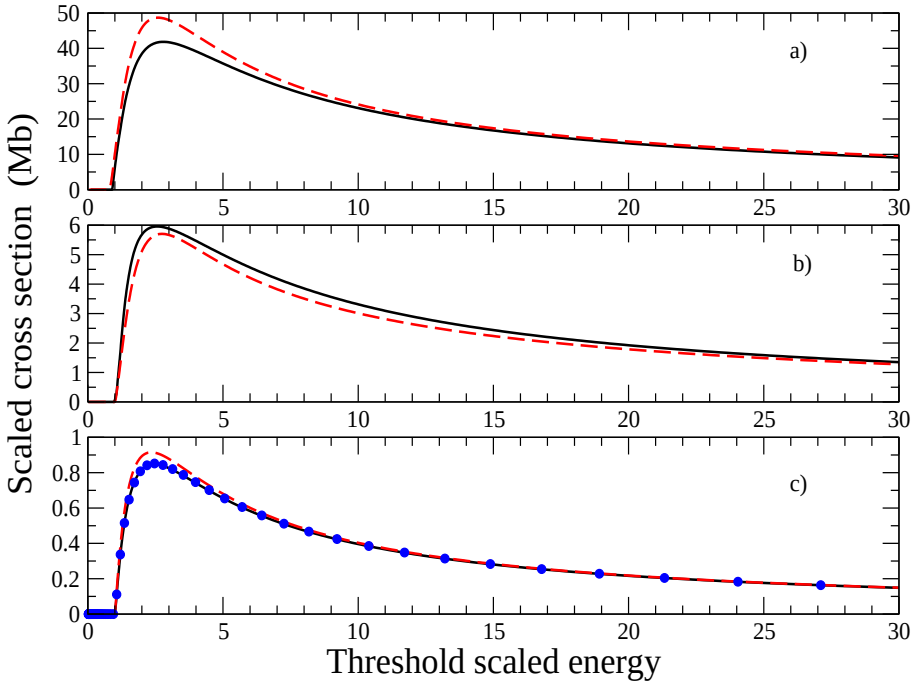

Figure 4. Electron-impact-ionization cross sections divided by n^4 vs threshold scaled energy for the n-bundled excited states of (a) B, (b) B^+,and (c)B^{2+}. In all plots the solid line shows the n = 3 RMPS data, the dashed line shows the n = 4 RMPS data and in panel (c) the solid circles show the n = 5 RMPS data (1 Mb = 10^{18} cm^2). Figure taken from [11]

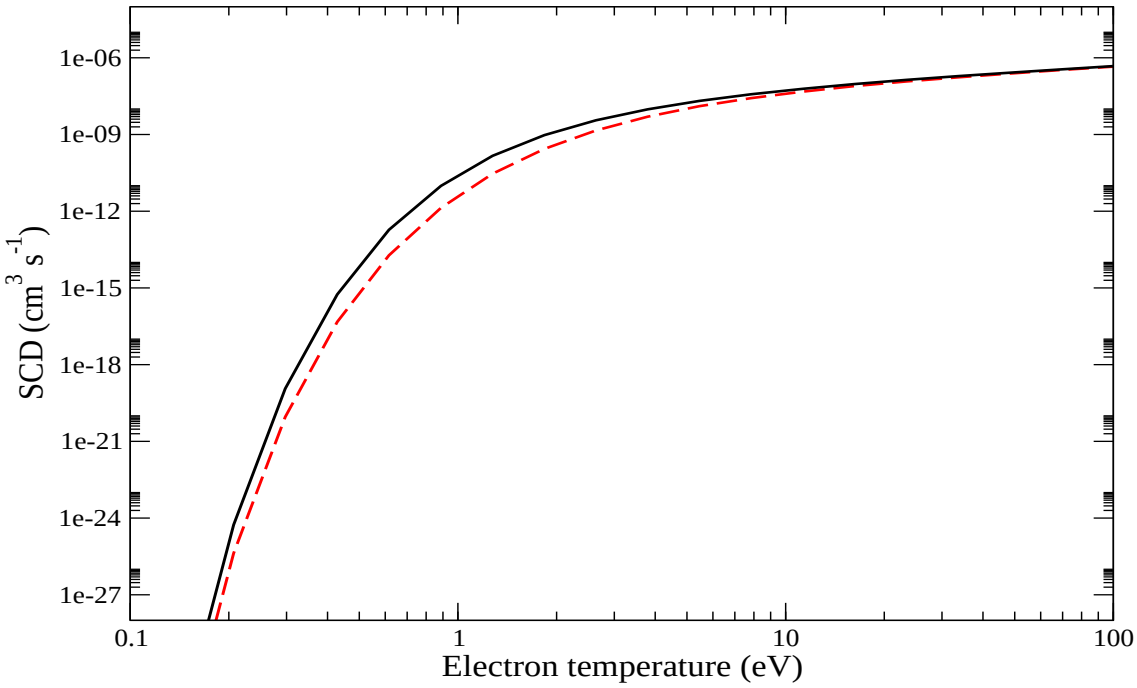

Figure 5. Effective ionization rate coefficient for B at a density of N_e=1 × 10^6 cm^{-3} (dashed line) and N_e=1 × 10^{14} cm^{-3} (solid line).

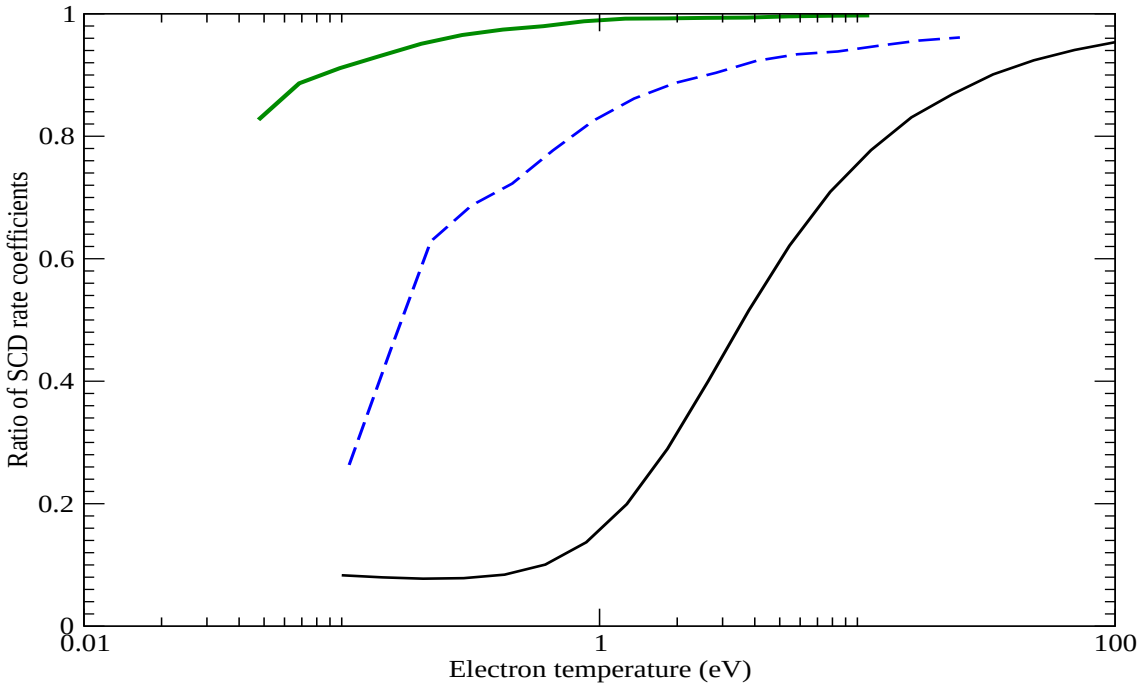

Figure 6. Ratio of the effective ionization rate coefficient at N_e=1 × 10^6 cm^{-3} to the value at N_e=1 × 10^{14} cm^{-3}. The lowest line shows the results for B, the dashed line shows the results for B^+ and the upper solid line shows the results for B^{2+}.